Atmos. Chem. Phys., 12, 10239–10255, 2012
www.atmos-chem-phys.net/12/10239/2012/
doi:10.5194/acp-12-10239-2012

Atmospheric Chemistry and Physics

Mixing state and compositional effects on CCN activity and droplet growth kinetics of size-resolved CCN in an urban environment

L. T. Padró[1,*], R. H. Moore[1], X. Zhang[2], N. Rastogi[2,], R. J. Weber[2], and A. Nenes[1,2]**

[1]School of Chemical and Biomolecular Engineering, Georgia Institute of Technology, Atlanta, GA, USA
[2]School of Earth and Atmospheric Sciences, Georgia Institute of Technology, Atlanta, GA, USA
[*]present address: Department of Civil and Environmental Engineering, Tufts University, Medford, MA, USA
[**]present address: Physical Research Laboratory, Ahmedabad, India

Correspondence to: A. Nenes (athanasios.nenes@gatech.edu)

Received: 22 September 2011 – Published in Atmos. Chem. Phys. Discuss.: 12 December 2011
Revised: 16 October 2012 – Accepted: 22 October 2012 – Published: 6 November 2012

Abstract. Aerosol composition and mixing state near anthropogenic sources can be highly variable and can challenge predictions of cloud condensation nuclei (CCN). The impacts of chemical composition on CCN activation kinetics is also an important, but largely unknown, aspect of cloud droplet formation. Towards this, we present in-situ size-resolved CCN measurements carried out during the 2008 summertime August Mini Intensive Gas and Aerosol Study (AMIGAS) campaign in Atlanta, GA. Aerosol chemical composition was measured by two particle-into-liquid samplers measuring water-soluble inorganic ions and total water-soluble organic carbon. Size-resolved CCN data were collected using the Scanning Mobility CCN Analysis (SMCA) method and were used to obtain characteristic aerosol hygroscopicity distributions, whose breadth reflects the aerosol compositional variability and mixing state. Knowledge of aerosol mixing state is important for accurate predictions of CCN concentrations and that the influence of an externally-mixed, CCN-active aerosol fraction varies with size from 31 % for particle diameters less than 40 nm to 93 % for accumulation mode aerosol during the day. Assuming size-dependent aerosol mixing state and size-invariant chemical composition decreases the average CCN concentration overprediction (for all but one mixing state and chemical composition scenario considered) from over 190–240 % to less than 20 %. CCN activity is parameterized using a single hygroscopicity parameter, κ, which averages to 0.16 ± 0.07 for 80 nm particles and exhibits considerable variability (from 0.03 to 0.48) throughout the study period. Particles in the 60–100 nm range exhibited similar hygroscopicity, with a κ range for 60 nm between 0.06–0.076 (mean of 0.18 ± 0.09). Smaller particles (40 nm) had on average greater κ, with a range of 0.20–0.92 (mean of 0.3 ± 0.12). Analysis of the droplet activation kinetics of the aerosol sampled suggests that most of the CCN activate as rapidly as calibration aerosol, suggesting that aerosol composition exhibits a minor (if any) impact on CCN activation kinetics.

1 Introduction

The ability of aerosol particles to act as cloud condensation nuclei (CCN) depends on their size and composition (e.g., Twomey, 1977; Dusek et al., 2006; Wang, 2007). Chemical composition can have an important effect on CCN, especially in environments where the aerosol is externally mixed (e.g., Cubison et al., 2008; Furutani et al., 2008). Köhler theory (Köhler, 1936) has been shown to adequately describe the size and compositional dependence of CCN composed of inorganic and soluble organic compounds (e.g., Cruz and Pandis, 1997; Padró et al., 2007). CCN containing higher molecular weight organic compounds can readily form cloud droplets but may exhibit more complex interactions with water, owing to their partial solubility in water, and ability to depress surface tension and create polymer networks (e.g., Li et al., 1998; Facchini et al., 1999; Corrigan and Novakov, 1999; Raymond and Pandis, 2002; Hartz et al., 2006; Petters et al., 2009). Despite this complexity, simple assumptions on the chemical composition of aerosols is often employed in modeling CCN. The ultimate test of these simplified models

are CCN closure studies, where measured CCN concentrations and predictions from Köhler theory are directly compared, where closure is deemed successful when agreement is found to be within the measurement uncertainty (typically 10–20 %).

Over the past decades, numerous closure studies have been carried out at a number of ground sites (e.g., Bigg, 1986; Liu et al., 1996; Covert et al., 1998; Cantrell et al., 2001; Roberts et al., 2002; Dusek et al., 2003; Roberts et al., 2003; Snider et al., 2003; Rissler et al., 2004; Broekhuizen et al., 2006; Chang et al., 2007; Ervens et al., 2007; Medina et al., 2007; Stroud et al., 2007; Vestin et al., 2007; Yum et al., 2007; Cubison et al., 2008; Kuwata et al., 2008; Bougiatioti et al., 2009; Gunthe et al., 2009; Chang et al., 2010; Kammermann et al., 2010; Rose et al., 2010; Wang et al., 2010; Rose et al., 2011), ships (e.g., Zhou et al., 2001, Quinn et al., 2008), and airborne platforms (e.g., Chuang et al., 2000; Van-Reken et al., 2003; Rissman et al., 2006; Roberts et al., 2006, 2010; Wang et al., 2008; Lance et al., 2009; Murphy et al., 2009; Asa-Awuku et al., 2011; Moore et al., 2011) throughout the world to address the effects of chemical composition and mixing state on CCN activity. Chemical composition data for CCN closures have been obtained from filters (Liu et al., 1996; Chuang et al., 2000), MOUDI (Micro Orifice Uniform Deposit Impactor) cascade impactors (Cantrell et al., 2001; Roberts et al., 2002, 2003; Bougiatioti et al., 2009), inferred from hygroscopic growth measurements (Covert et al., 1998; Zhou et al., 2001; Rissler et al., 2004; Ervens et al., 2007; Vestin et al., 2007), Particle-Into-Liquid-Samplers (PILS; Kuwata et al., 2008) and aerosol mass spectrometers (AMS; Broekhuizen et al., 2006; Medina et al., 2007; Stroud et al., 2007; Cubison et al., 2008; Lance et al., 2009; Murphy et al., 2009; Gunthe et al., 2009). CCN closure utilizing AMS measurements tend to be more successful (typically within 20–50 %), due to its fast time resolution ($\sim$1 Hz) and ability to resolve size-dependant composition. CCN closure in remote environments that use filter-based methods have nevertheless given exceptionally good closure (on the order of a few percent; Bougiatioti et al., 2009, 2011).

Although introducing size-dependent chemical composition (Medina et al., 2007; Stroud et al., 2007; Cubison et al., 2008; Gunthe et al., 2009; Murphy et al., 2009) and accounting for the aerosol mixing state (Broekhuizen et al., 2006; Cubison et al., 2008; Lance et al., 2009) have been found to improve CCN closure, it is still unclear the extent of error associated with ignoring such information in simulations of the aerosol indirect effect. For example, Ervens et al. (2007) found that knowing the mixing state of the aerosol is more important to achieve closure than the size-dependent aerosol chemical composition; while other studies (e.g., Medina et al., 2007; Lance et al., 2009; Asa-Awuku et al., 2011) have found that knowledge of both chemical composition and mixing state are required to achieve closure to within 10–20 %. The treatment of organics in Köhler theory can be described with single-parameter approaches (e.g., Petters and Kreidenweis, 2007), but will nevertheless be subject to some uncertainty and possibly contribute to the discrepancy between measurements and predictions when organics dominate the aerosol mass fraction (e.g., Moore et al., 2011). Rissman et al. (2004) and Sotiropoulou et al. (2007) have shown that even when CCN prediction errors are large, the uncertainty in cloud droplet number associated with these errors is substantially reduced by at least 50 %. If the CCN prediction error is on the order of 20 % as suggested in recent studies (Medina et al., 2007) it may not contribute a significant source of error in the assessment of the aerosol indirect effect (Sotiropoulou et al., 2007). However in regions where aerosol is externally mixed, the CCN prediction uncertainty can be high enough to yield important cloud droplet number prediction uncertainty (Karydis et al., 2012).

Another uncertain aspect of cloud droplet formation is the potential impact of slowly-dissolving compounds, droplet surface forming films and aerosol amorphous/glassy states on the activation kinetics of CCN. If present, kinetic activation delays could have an important impact on cloud droplet number and size distribution (e.g., Chuang et al., 1997; Nenes et al., 2001; Feingold and Chuang, 2002; Lance et al., 2004). To test whether such limitations exist, in-situ field studies compare the size of the activated droplets from the CCN being studied against those obtained from calibration salt aerosol known to exhibit rapid activation kinetics (e.g., Sorooshian et al., 2008; Bougiatioti et al., 2009, 2011; Lance et al., 2009; Murphy et al., 2009; Padró et al., 2010; Cerully et al., 2011). The difference in droplet sizes can reveal whether the compounds present in the aerosol retard droplet growth (i.e., growth kinetics is slower than expected from gas-to-particle transfer of water vapor). Many studies using this method of Threshold Droplet Growth Analysis (TDGA) have found little or no evidence of slow droplet growth kinetics (e.g., Bougiatioti et al., 2009, 2011; Lance et al., 2009; Padró et al., 2010; Cerully et al., 2011), although others have detected the occurrence of slow kinetics for organic-rich aerosol (e.g., Sorooshian et al., 2008; Murphy et al., 2009). When combined with a computational fluid dynamics model of the CCN instrument (Lance et al., 2006; Lathem et al., 2011; Raatikainen et al., 2012), changes in growth kinetics can be parameterized in terms of an uptake coefficient (Asa-Awuku et al., 2009; Engelhart et al., 2008; Ruehl et al., 2008, 2009; Moore et al., 2012; Raatikainen et al., 2012).

This paper presents size-resolved CCN and droplet growth kinetic measurements obtained during a ground site study in Atlanta, Georgia, during August and September of 2008. This work complements an emerging number of studies that use size-resolved CCN measurements to infer the compositional dispersion and the processes that affect aerosol hygroscopicity (e.g., Lance, 2007; Gunthe et al., 2009; Rose et al., 2010; Mochida et al., 2010; Irwin et al., 2011; Bougiatioti et al., 2011; Su et al., 2010; Cerully et al., 2011; Lance et al., 2012). The data presented here correspond to an environment

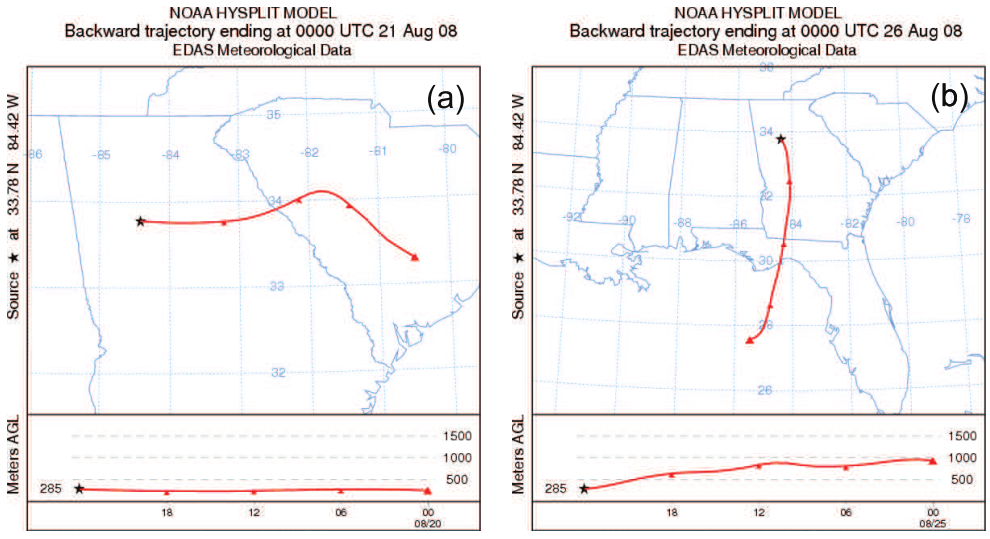

Fig. 1. HYSPLIT one day back-trajectories representative of the air masses sampled in JST during the AMIGAS campaign. **(a)** represents a "period A" air mass originating from the continental US; while **(b)** represents a "period B" air mass which originated from the Gulf of Mexico. During 24 August till the 27th, the air masses originated either from the Atlantic Ocean or the Gulf of Mexico.

where fresh anthropogenic (urban) emissions interact with biogenic emissions from forested areas prevalent throughout the southeastern United States, producing aerosol that strongly forces regional climate (Goldstein et al., 2009). Apart from deriving size-resolved hygroscopicity distributions, this study focuses on comparing in-situ CCN concentrations against predicted concentrations from the observed size distributions and chemical composition. A number of simplifying compositional and mixing state assumptions are used (typical of what is adopted in climate models when calculating CCN concentrations), and the associated CCN prediction errors are quantified. Finally, this study also focuses on the droplet growth kinetics of urban aerosols by comparing the droplet size of the atmospheric CCN to those of $(NH_4)_2SO_4$ calibration aerosol.

2 Data set description

2.1 Measurement site

The main objective of the 2008 August Mini Intensive Gas and Aerosol Study (AMIGAS) campaign was to study the interactions between biogenic and anthropogenic emissions and how these impact secondary organic aerosol (SOA) formation. Atlanta was chosen for the study site since it represents a typical urban environment, but with strong biogenic influences (Weber et al., 2003). The major components of PM mass in Atlanta aerosol are sulfate and organic carbon (OC) with mostly OC in the ultrafine particle size mode (Butler et al., 2003; Rhoads et al., 2003; Solomon et al., 2003). When aerosol composition is dominated by OC, formation mechanisms are most likely due to local sources; while periods when the particles are dominated by sulfate result from the photochemical production from sources outside of Atlanta such as power plants (Weber et al., 2003).

The measurements presented in this study were obtained during 1 August 2008–15 September 2008 at the Jefferson Street site (JST) in downtown Atlanta (33.777° N, 84.416° W), which is affected by fresh urban and regional emissions. Measurements were performed during the summer season since it is the period where SOA is more abundant and mostly formed from biogenic precursors (Lim and Turpin, 2002; Weber et al., 2007; Hennigan et al., 2009).

HYSPLIT back-trajectories (www.arl.noaa.gov/ready/hysplit4.html) were used to determine the characteristics and origin of the air masses affecting JST throughout the campaign. Two characteristic periods with different air mass types were identified (Fig. 1). Period A is affected by "polluted" air masses that originate from the continental United States (1–20 August and 28 August–15 September); while Period B is influenced by "cleaner" air masses that originate either from the Atlantic Ocean or the Gulf of Mexico (21–27 August). Period B was also characterized by precipitation events that considerably reduced particle concentrations through wet deposition processes (although some rain events also occurred occurred during Period A, these were not as strong and widespread as those observed in Period B). The effect of different air masses and precipitation events on JST site is evident in the total particle (condensation nuclei, CN) and CCN concentrations, (Fig. 2a) which during Period B decrease and are statistically different (at the 99 % confidence level) from Period A concentrations.

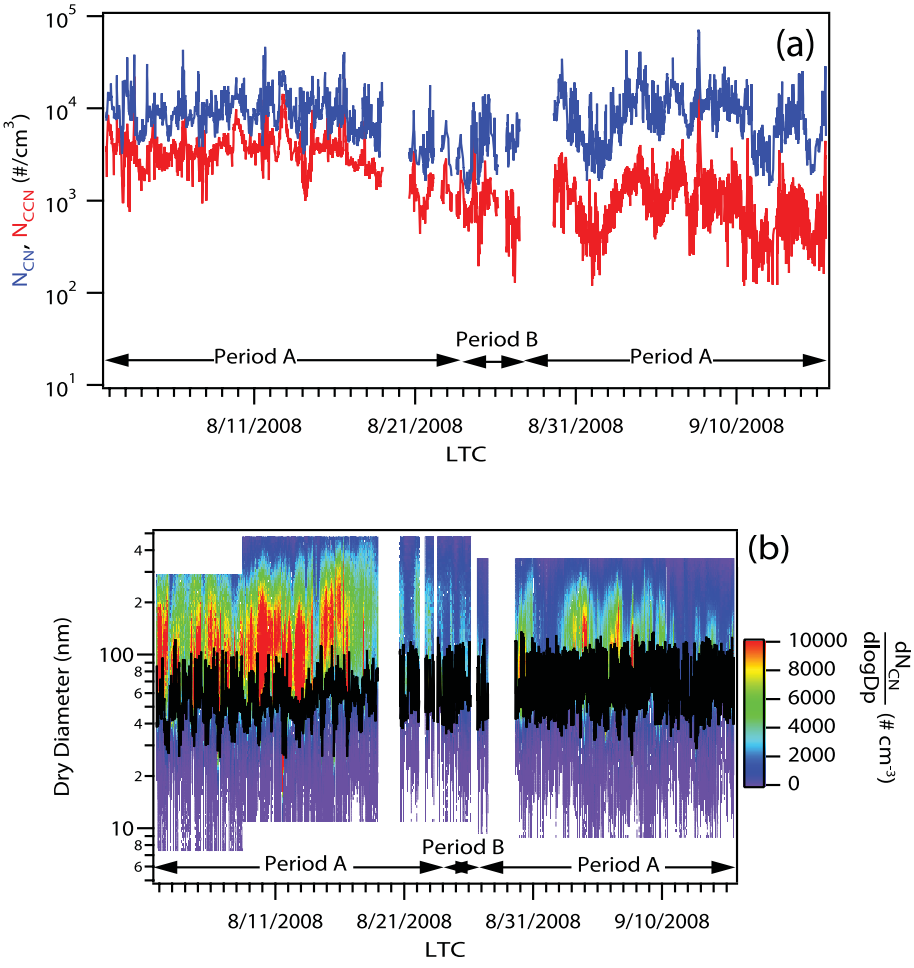

Fig. 2. (a) Total CN and CCN time-series (for all five supersaturations studied during the AMIGAS campaign) for whole AMIGAS campaign. **(b)** Particle size distribution time-series with characteristic dry diameter, $d_{p,c}$ (black line). Period A corresponds to "polluted" air masses originating from the continental US; period B corresponds to "cleaner" air masses originating from either the Atlantic Ocean or Gulf of Mexico. Gaps in data are a result of instrument outage.

2.2 Chemical composition measurements

Two particle-into-liquid-samplers (PILS) were used to study bulk aerosol composition; one for real-time measurement of ionic composition (using ion chromatography; IC), and one for water-soluble organic carbon (WSOC). Coarse size aerosols (2.5 µm aerodynamic diameter and above) were removed from the sample air stream with a cyclone. In each PILS, the aerosols are exposed to supersaturated water vapor and nucleate droplets that are subsequently collected on a plate via inertial impaction. A purified water stream flows over the plate and the solution stream is then sent to the analytical instrumentation. The PILS-IC (Weber et al., 2001) uses a dual channel Ion Chromatograph (Dionex Model 300DX), which allows the detection of Ca^{2+}, Mg^{2+}, K^+, Na^+, Cl^-, NH_4^+, NO_3^-, NO_2^-, SO_4^{2-}, formate, and oxalate ions integrated over roughly 3 min of sampling with measurements repeated every 20 min. The PILS-WSOC (Sullivan et al., 2004) uses a Sievers Model 800 Turbo Total Organic Carbon (TOC) Analyzer to obtain the aerosol WSOC mass. Before the WSOC measurements are performed, the sample stream is filtered to remove any large insoluble particles. The PILS-WSOC reports the soluble organic concentration by integrating over 10 min. Both types of chemical composition measurements are used for predicting aerosol hygroscopicity as described in Sect. 3.3.

2.3 Size-resolved CCN and particle concentrations

A Scanning Mobility Particle Sizer (SMPS) was used to measure the particle size distribution for particles having electrical mobility diameters (d_m) ranging from 7 to 500 nm. The SMPS consists of a Differential Mobility Analyzer (DMA; TSI Model 3081) running in series with a Condensation Particle Counter (CPC; TSI Model 3022A or TSI Model 3010). Prior to classification, aerosols are passed through a Kr-85

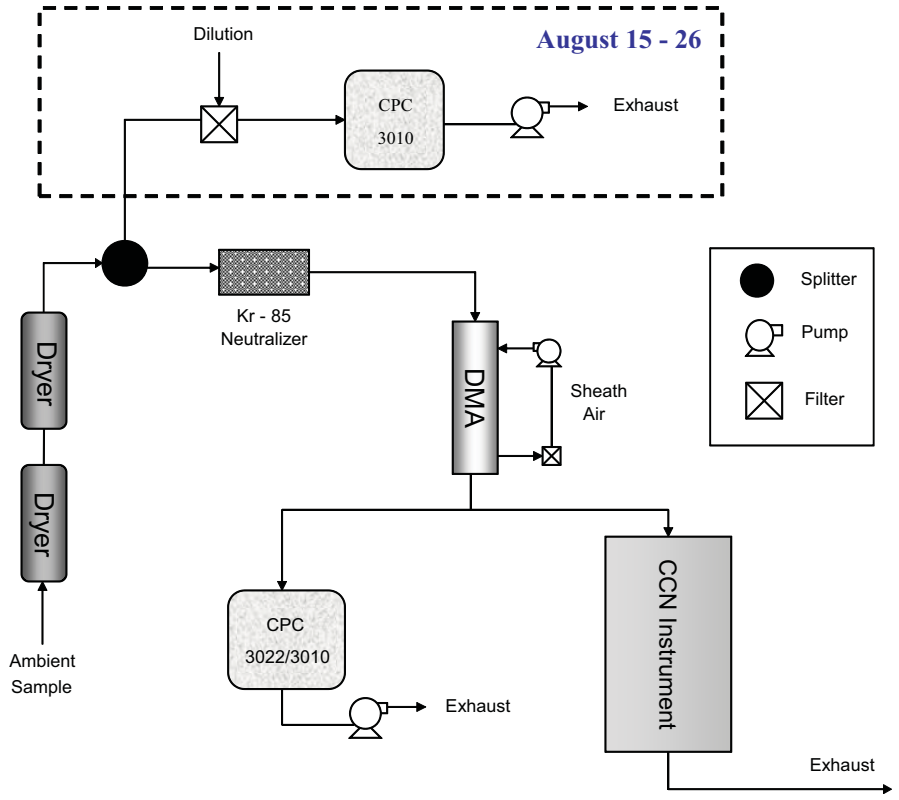

Fig. 3. AMIGAS experimental set up. From 1 till 26 August, the CPC 3022A was used for the SMPS; while the CPC 3010 was used from 26 August till the end of the campaign (15 September). The sheath-to-aerosol ratio in the DMA was run at 10:1 (1 till 8 August; Setup A1) and 5:1 (8 August till 15 September; Setup A2 and B). The dotted box highlights the total CN measurement which was done from 15 till 26 August with the CPC3010.

bipolar charger to acquire an equilibrium charge distribution. The charged particles are then classified by the DMA, and sent to a CPC to measure the total aerosol number concentration, and a Continuous-Flow Streamwise Thermal Gradient CCN Chamber (CFSTGC; Roberts and Nenes, 2005; Lance et al., 2006) to measure the number of particles that act as CCN (discussed in Sect. 2.4). By scanning the DMA voltage, a complete particle size distribution is obtained in two minutes. During the course of the study, two different CPCs and DMA sheath-to-aerosol ratios were used. The first CPC (TSI Model 3022A) was replaced on 26 August with a TSI Model 3010 due to an equipment malfunction. Adjustment of the DMA sheath-to-aerosol flow from 10:1 to 5:1 was made on 8 August in order to improve aerosol counting statistics from a broader DMA transfer function. Overall, three SMPS setups (Fig. 3) were employed to optimize counting statistics with the new flow rates. Setups A1 and A2 have a CPC 3022A and sheath-to-aerosol ratios of 10:1 and 5:1, respectively; while setup B has a CPC 3010 and a 5:1 sheath-to-aerosol ratio. Particles sampled were assumed to be spherical, which is supported by previous aerosol measurements in Atlanta (McMurry et al., 2002).

An intercomparison between the 3022 and 3010 CPCs was carried out by comparing the total CN concentration measured by each instrument for data collected between 15 August and 26 August (Fig. 3; Setup A2). As both CPCs have different particle size detection limits (7 nm and 10 nm for the CPC 3022 and CPC 3010, respectively), the particle size distribution obtained from the SMPS (that used the 3022 as a particle detector) was integrated above 10 nm to match the size range of the CPC 3010. The data were filtered to include only scans for which aerosol modes are fully resolved within the dynamic range of the scan, and, where the total CN remains constant throughout the scan (within 15 % of average CN concentration). Furthermore, periods of exceptionally high total CN concentrations ($>10^4$ particles cm^{-3}), were removed from the data to avoid coincidence errors associated with the CPC 3010. Based on the measurements, the integrated size distributions with the CPC 3022 were found to be about 25 % lower than the CN concentration from the CPC 3010. About 15 % of this bias could be attributed to instrument-dependent bias (determined by sampling the same air mass with both instruments). The absolute bias varied approximately linearly with concentration with a negligible constant bias, while the relative bias remained

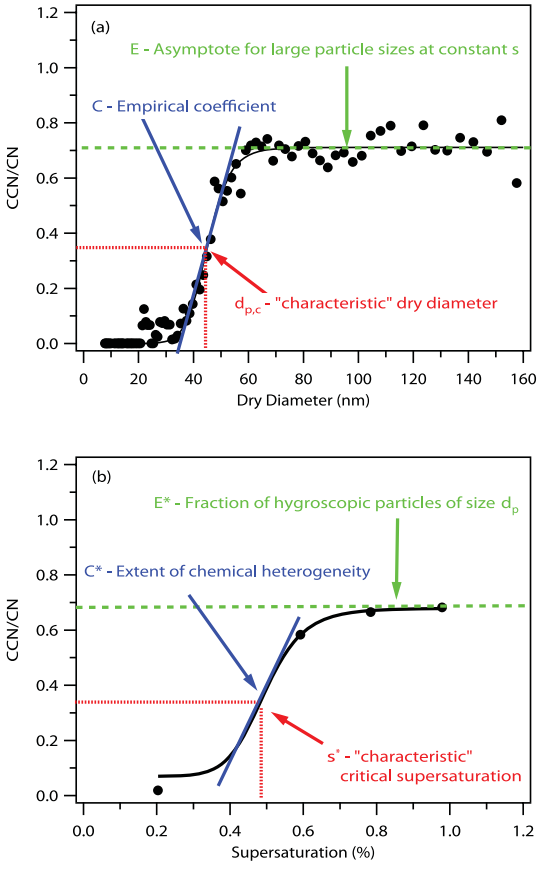

Fig. 4. (a) Example of the CCN-to-CN activation ratio as a function of dry diameter (for $s = 0.98\,\%$ on 2 August 2008 at 01:30 a.m.) with sigmoid fit and its defined parameters. **(b)** Example of CCN-to-CN activation ratio as a function of supersaturation for a 80 nm dry particle (sample collected on 14 August 2008 at 01:00 p.m.) as derived from the SMCA with sigmoid fit and its defined parameters.

constant. The total CN concentrations (measured and predicted) obtained for Setups A1 and A2 were corrected for this bias before the CCN closure analysis was performed. The total CN time-series (after correction) is shown in Fig. 2a. Throughout the campaign the CCN was found to correlate well with the CN concentration and increased with supersaturation (Fig. 2a).

The total aerosol concentration was measured continuously with a CPC with a detection diameter of 10 nm (TSI model 3010) from 15 August to 26 August. Apart from providing a consistency check the separate CPC was used to detect small intense plumes that may occasionally pass over the site that could not be resolved with the 120s scantime of the SMPS.

2.4 CCN measurements

Prior to measurement, the sampled air stream was dried from ambient relative humidity (RH) to ~21 % RH to minimize residual water, as this can affect the inference of aerosol CCN activity, especially for very acidic aerosol (e.g., Murphy et al., 2009). The classified aerosol was sent to the CFSTGC chamber, where some particles activate to form droplets and counted by an optical particle counter (OPC) at the end of the growth chamber. The OPC also sizes the activated droplets, ranging from ~1 to 10 µm with a resolution of 0.5 µm.

In this work, size-dependant CCN activity data is obtained using Scanning Mobility CCN Analysis (SMCA; Moore et al., 2010). In SMCA, the DMA voltage is exponentially scanned over time (120 s upscan, 15 s downscan) to continuously sample particles across the size distribution. The time-series of CCN and CN counts are then inverted to obtain size-resolved CCN concentration and activated droplet size. The aerosol size, analyzed for this study, ranged from 10 to 500 nm, depending on the sheath-to-aerosol ratio used in the DMA (10:1 or 5:1). A total of five supersaturations (s) were applied in the following order: 0.2, 0.6, 1.0, 0.8, and 0.4 % supersaturation, allowing sufficient time (6 min) for the instrumentation to reach steady state following a supersaturation change. Instrument supersaturation was calibrated with classified $(NH_4)_2SO_4$ particles using a similar procedure to that of Rose et al. (2008) and Padró et al. (2010).

3 Experimental analysis

The CCN activity of the aerosol is characterized at each supersaturation by determining the "critical" dry particle diameter, $d_{p,c}$, above which particles activate to form droplets. Operationally this is defined as the dry diameter for which the CCN to CN ratio equals 0.50 (assuming all CN are CCN active at a specific supersaturation). As shown in Fig. 4a, the sigmoidal activation curve can be used to infer the $d_{p,c}$. From this size-resolved data, the mixing state and hygroscopicity parameter distribution are determined (Sect. 3.1).

CCN activation kinetics are determined from the CCN measurements by monitoring the change in droplet size measured by the OPC for all supersaturations and dry particle diameters considered, and by comparing these sizes to those for $(NH_4)_2SO_4$ calibration particles with the same critical supersaturation.

3.1 Analysis of SMCA data

Each DMA size scan was screened for fluctuations in the CFSTGC chamber temperature gradient, OPC temperature, and stability of the flows. Data exhibiting maximum temperature or flow deviations of more than 15 % from the setpoint were discarded. The size-dependent activation ratio function, $R_d(d_p, s)$, was determined by computing the CCN to CN ratio as a function of dry particle diameter, d_p, at constant supersaturation s. $R_d(d_p, s)$ was fit to a sigmoidal curve:

$$R_d(d_p, s) = \frac{N_{CCN}(d_p, s)}{N_{CN}(d_p)} = \frac{E}{1 + \left(\frac{d_{p,c}}{d_p}\right)^c} \quad (1)$$

where N_{CCN} is the total CCN number concentration, N_{CN} is the total aerosol number concentration, E is the asymptote of $R_d(d_p, s)$ at large particle sizes, $d_{p,c}$ is the characteristic dry diameter for which most particles are CCN and corresponds to the inflection point of the sigmoid, and c is an empirical coefficient that captures the slope of the sigmoidal function (Fig. 4a). Overall, we found Eq. (1) to describe the size-resolved CCN well (e.g., Fig. 4a). However, in some cases integrating the fitted sigmoids did not reproduce the measured CCN concentration within 15 % and therefore were removed from the analysis.

$R_d(d_p, s)$ can be used to study the size-dependent hygroscopicity and mixing state by evaluating the function at different diameters (in this study, at 30, 40, 50, 60, 70, 80, 90, and 100 nm) for all sigmoids within a supersaturation cycle. The supersaturation-dependant activation ratio function, $R_a(s, d_p)$, (the fraction of particles of size d_p that are CCN at s) is subsequently determined and fit to a new sigmoidal function (Bougiatioti et al., 2011):

$$R_a(s, d_p) = \frac{N_{CCN(s, d_p=const)}}{N_{CN(d_p=const)}} = \frac{E^*}{1 + \left(\frac{s}{s^*}\right)^{c^*}} \quad (2)$$

where E^* is the asymptotic activated fraction at large supersaturations, s^* is the characteristic critical supersaturation of particles with diameter d_p, and c^* is a fitting constant that captures the slope of the fitting function (which is related to aerosol chemical heterogenity). Figure 4b shows a typical example of $R_a(s, d_p)$ for 80 nm particles obtained on 14 August.

As described by Lance (2007), Bougiatioti et al. (2011), and Cerully et al. (2011), $R_a(s, d_p)$ mostly reflects the cumulative distribution of the "characteristic" critical supersaturation for particles of constant d_p, and can be expressed as a cumulative distribution of hygroscopicity, $R_a(\kappa)$, as follows. Assuming that $R_a(\kappa)$ is driven solely by the chemical composition variance and using the asymptotic expression of κ for high hygroscopicity (Petters and Kreidenweis, 2007),

$$\kappa = \frac{4A^3}{27 d_{50}^3} s^{-2} \quad (3)$$

where $A = \frac{4 M_w \sigma_w}{RT\rho_w}$ (Petters and Kreidenweis, 2007), R is the ideal gas constant, T is the temperature and M_w, σ_w, ρ_w are the molar mass, surface tension, and density of water, respectively. For every s^* there is a corresponding "characteristic" hygroscopicity parameter, κ^*, so that (s/s^*) can be expressed as $(\kappa/\kappa^*)^{-1/2}$. Substituting this into Eq. (2) gives $R_a(\kappa)$, which is the fraction of particles of size d_p that are CCN as a function of κ:

$$R_a(\kappa) = \frac{E^*}{1 + \left(\frac{\kappa}{\kappa^*}\right)^{c^*/2}} \quad (4)$$

Differentiating and normalizing Eq. (4) gives the probability distribution of κ, $p(\kappa)$, for particles of constant size (Lance, 2007; Bougiatioti et al., 2011; Cerully et al., 2011),

$$p(\kappa) = \frac{1}{E^*}\frac{dR_a(\kappa)}{d\kappa} = \frac{c^*}{2\kappa^*} \frac{\left(\frac{\kappa}{\kappa^*}\right)^{\frac{c^*}{2}-1}}{\left(1 + \left(\frac{\kappa_*}{\kappa}\right)^{\frac{c^*}{2}}\right)^2} \quad (5)$$

from which one can compute the variance of the distribution function, which represents the extent of aerosol chemical heterogeneity within the CCN-active aerosol fraction,

$$\sigma_\kappa^2 = \frac{\int_0^1 (\kappa - \kappa^*)^2 p(\kappa) d\kappa}{\int_0^1 p(\kappa) d\kappa} \quad (6)$$

The upper limit of hygroscopicity in the integrals is operationally set to unity, which captures the upper limit of atmospheric κ values in the absence of sea salt (Cerully et al., 2011). κ and σ_κ are obtained for all diameters and supersaturations considered.

3.2 CCN distribution

Since the size-resolved aerosols are sent simultaneously to the CPC and CCN counter for CN and CCN measurements, the CCN distribution can be obtained by multiplying the particle size distribution with the $R_d(d_p, s)$ ratio. The CCN distribution at a given supersaturation, $\frac{dN_{CCN}}{d\log d_p}$, is defined as:

$$\frac{dN_{CCN}}{d\log d_p} = R_d(d_p, s) n(d_p) \quad (7)$$

where $n(d_p)$ is the particle size distribution. Substituting Eq. (1) into Eq. (7) gives:

$$\frac{dN_{CCN}}{d\log d_p} = \frac{E}{1 + \left(d_{p,c}/d_p\right)^c} n(d_p) \quad (8)$$

Integrating Eq. (8) for all sizes gives the total CCN concentration (N_{CCN}) in cm^{-3}:

$$N_{CCN} = \int_0^\infty \frac{dN_{CCN}}{d\log d_p} d\log d_p. \quad (9)$$

It should be emphasized that the supersaturation in Eqs. (7)–(9) is kept constant.

3.3 CCN closure and mixing state

CCN closure refers to a comparison between measured and predicted CCN concentrations. CCN closures are performed to determine how well Köhler theory can predict CCN concentrations when the chemical composition and mixing state of the aerosol are known. It can also be used to quantify the errors associated with simplifying assumptions taken to calculate CCN concentrations in atmospheric models. To predict CCN concentrations, the supersaturation, the aerosol

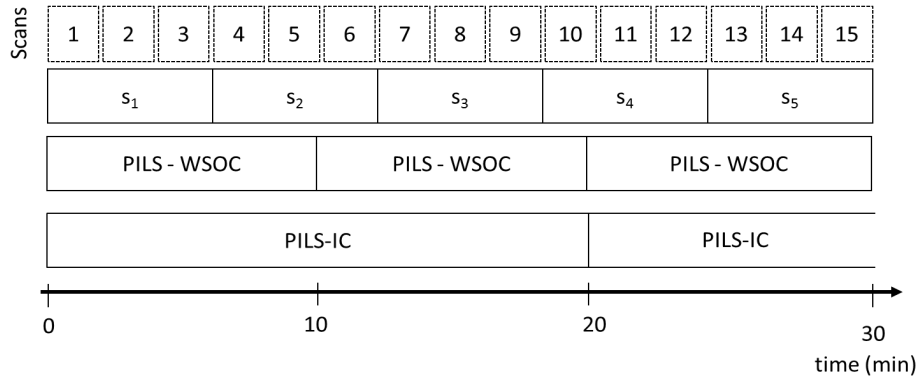

Fig. 5. Coordination of measurements used in this study for each 30 min measurement cycle. *s* is the symbol for "supersaturation"; PILS-WSOC, PILS-IC stand for "Particle-In-Liquid-Sampler" for water soluble organic carbon and inorganic ions, respectively.

size distribution, and aerosol chemical composition (bulk or size resolved) are needed. CCN predictions were made using the measured CN size distributions (120 s resolution) and bulk particle chemical composition information from the PILS-IC (20 min resolution) and PILS-WSOC (620 s resolution). The chemical composition data was binned to match the SMCA time series as shown in Fig. 5 to account for the diversity of measurement frequency of each instrument.

The predicted CCN concentration at each supersaturation was determined by calculating the minimum aerosol diameter that acts as a CCN, termed "activation diameter", $d_{\mathrm{p,c}}$, from Köhler theory (Köhler, 1936):

$$d_{\mathrm{p,c}} = \left(\frac{256 M_{\mathrm{w}}^3 \sigma^3}{27 R^3 T^3 \rho_{\mathrm{w}}^3}\right)^{1/3} \left[\sum_i \left(\frac{M_{\mathrm{w}}}{\rho_{\mathrm{w}}}\right)\left(\frac{\rho_i}{M_i}\right)\varepsilon_i \upsilon_i\right]^{-1/3} s^{-2/3} \quad (10)$$

where σ is the surface tension of the CCN at the point of activation (here assumed to be equal to σ_{w}, unless otherwise specified) and ρ_i, ε_i, υ_i, and M_i are the density, volume fraction, effective van't Hoff factor and molar mass of the solute i (sulfuric acid, ammonium bisulfate, ammonium sulfate, ammonium nitrate, and organic species). The volume fraction of solute i in the dry particle, ε_i, is related to its mass fraction, x_i, as:

$$\varepsilon_i = \frac{x_i/\rho_i}{\sum_j (x/\rho)_j} \quad (11)$$

For the closure, the effective van't Hoff factor of organic species was assumed to be 1, while the Pitzer activity coefficient model (Pitzer and Mayorga, 1973; Pilinis and Seinfeld, 1987; Clegg and Brimblecombe 1988) was used to calculate the effective van't Hoff factor of all inorganic salts present in the sample, at the concentration corresponding to the critical wet droplet diameter of the CCN. The PILS–IC data is then used to determine the inorganic salts present in the dry aerosol. The ions present are (almost exclusively) ammonium, sulfate and nitrate. Following Nenes et al. (1998), the sulfate molar ratio, $R_{\mathrm{SO_4}} = [\mathrm{NH_4^+}]/[\mathrm{SO_4^{2-}}]$, was used to determine the types of sulfate salts present in the dry aerosol. When $R_{\mathrm{SO_4}} \leq 1$, the sulfate and ammonium are present as a mixture of H_2SO_4 and NH_4HSO_4; when $1 < R_{\mathrm{SO_4}} < 2$, the sulfate and ammonium are present as a mixture of NH_4HSO_4 and $(NH_4)_2SO_4$ and when $R_{\mathrm{SO_4}} \geq 2$, the sulfate and ammonium are present as $(NH_4)_2SO_4$ and NH_4NO_3. A mass balance on the PILS–IC measurements determines the amounts of each salt. Organics in the aerosol are determined from the PILS–WSOC.

Two different CCN closure schemes were assessed based on assumptions related to the chemical composition and mixing state of the aerosol (i.e., the maximum activated fraction, E, obtained from the CCN spectrum):

- *Internal Mixture (INT)* – all particles have the same composition.
- *External Mixture (EXT)* – two types of particles are present: soluble particles and insoluble particles. Only the soluble particles contribute to the CCN; the relative number fraction of soluble particles is E, and $(1 - E)$ are considered insoluble.

In addition to the different aerosol mixing states a number of different chemical composition and surface tension assumptions are explored for the soluble fraction:

- *Ammonium Sulfate (AS)* – the aerosol is assumed to be composed of pure $(NH_4)_2SO_4$. Although this scenario does not reflect the true composition of the aerosol, it corresponds to an upper hygroscopicity limit for continental aerosol.
- *Soluble Salts, Insoluble Organics (SALTS)* – here, only soluble inorganic salts are assumed to contribute solute. This scenario underestimates aerosol hygroscopicity because the organics are known to contain water-soluble compounds (as reflected in the PILS–WSOC observations); however, this case is still instructive as neglecting organic hygroscopicity is a common model assumption.

– *Soluble Salts, Soluble Organics (ALLSOL)* – the aerosol is composed of soluble inorganic salts and soluble organics, as determined from the PILS measurements. Contrary to the SALTS scenario, in this case all organics in the aerosol are treated as soluble (with $\upsilon_{org} = 1$, $M_{org} = 250\,g\,mol^{-1}$, $\rho_{org} = 1.4\,g\,cm^{-3}$), corresponding to a characteristic organic hygroscopicity $\kappa = 0.1$.

– *Soluble Salts, Soluble and Surface-Active Organics (ALLSOL-ST)* – the aerosol follows the *ALLSOL* scenario, with the added assumption that organic species present are assumed to be surface active and reduce the surface tension of the solution droplet to 75 % that of pure water (Padró et al., 2010).

The only soluble salts compositional case was only applied to the internal mixture case, while the other compositional assumptions were applied to both cases for a total of seven closure scenarios considered. Hereafter, the scenarios are referenced by combining the acronyms of the mixing state and composition scenario (e.g., *INT-AS* is internally-mixed aerosol composed only of ammonium sulfate).

The total CCN predicted from the seven CCN closure scenarios explained above are compared to the total CCN obtained from SMCA. The CCN closure is statistically assessed with a least-squares linear fit between observations and predictions. In addition, the closure agreement is assessed in terms of two error metrics: the Normalized Mean Error (NME) and the Normalized Mean Bias (NMB),

$$\mathrm{NME} = \frac{\sum_i^n |P_i - O_i|}{\sum_i^n O_i} \tag{12}$$

and

$$\mathrm{NMB} = \frac{\sum_i^n (P_i - O_i)}{\sum_i^n O_i} \tag{13}$$

where P and O are the predicted and measured "critical" dry particle diameter or total CCN number concentrations averaged over each SMPS scan, i. These metrics provide additional information regarding the accuracy and bias of the theoretical predictions.

The compositional scenarios defined above reflect the range of assumptions taken in atmospheric models for calculating CCN concentrations, and are used to help quantify the CCN prediction error associated with their application. An observationally-based mixing state closure calculation would also be relevant but cannot be carried out here due to lack of relevant data (e.g., Rhoads et al., 2003) over the observation period considered.

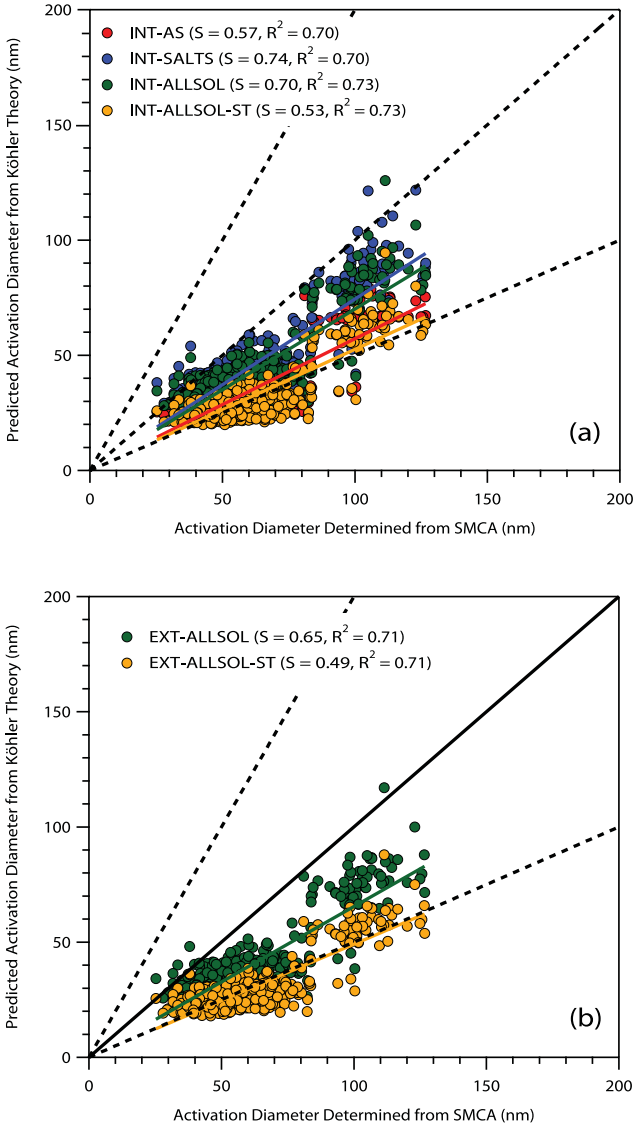

Fig. 6. (a) $d_{p,c}$ closure for the internal mixture (INT) scenarios. The red, blue, green, and yellow circles correspond to the INT-AS, INT-SALTS, INT-ALLSOL, and INT-ALLSOL-ST cases (Table 1), respectively. **(b)** $d_{p,c}$ closure for the external mixture (EXT) scenarios. The green and yellow circles correspond to the EXT-ALLSOL, and EXT-ALLSOL-ST cases (Table 1), respectively. Dashed lines represent 1:2 and 2:1 prediction error.

4 Results and discussion

4.1 CCN closure

Since the SMCA technique and the sigmoidal fit (Eq. 1) provide us with the characteristic activation diameter, a comparison between the measured and predicted $d_{p,c}$ can be performed. For the internal mixture case, a diameter comparison was done for the four chemical composition and surface tension scenarios (Table 1; Fig. 6a). For all scenarios

Table 1. "Critical" dry particle diameter closure analysis error metrics for entire AMIGAS campaign.

Description of CCN Closure Scenario	Linear Fit Slope (R^2)	Normalized Mean Error	Normalized Mean Bias
Internal Mixture – $(NH_4)_2SO_4$ (*INT-AS*)	0.57 (0.70)	0.428	−0.428
Internal Mixture – Only Salts Soluble (*INT-SALTS*)	0.74 (0.70)	0.273	−0.261
Internal Mixture – All Soluble (*INT-ALLSOL*)	0.70 (0.73)	0.307	−0.302
Internal Mixture – All Soluble and Surface Active (*INT-ALLSOL-ST*)	0.53 (0.73)	0.477	−0.477
External Mixture – $(NH_4)_2SO_4$ (*EXT-AS*)	N/A	N/A	N/A
External Mixture – All Soluble (*EXT-ALLSOL*)	0.65 (0.71)	0.349	−0.346
External Mixture – All Soluble and Surface Active (*EXT-ALLSOL-ST*)	0.49 (0.71)	0.509	−0.509
Size-Resolved – External Mixture (*SR-EXT*)	N/A	N/A	N/A

Table 2. CCN closure analysis error metrics for entire AMIGAS campaign.

Description of CCN Closure Scenario	Linear Fit Slope (R^2)	Normalized Mean Error	Normalized Mean Bias
Internal Mixture – $(NH_4)_2SO_4$ (*INT-AS*)	2.23 (0.32)	1.937	1.937
Internal Mixture – Only Salts Soluble (*INT-SALTS*)	1.96 (0.53)	1.462	1.462
Internal Mixture – All Soluble (*INT-ALLSOL*)	2.02 (0.48)	1.567	1.567
Internal Mixture – All Soluble and Surface Active (*INT-ALLSOL-ST*)	2.34 (0.33)	2.065	2.065
External Mixture – $(NH_4)_2SO_4$ (*EXT-AS*)	1.17 (0.64)	0.489	0.401
External Mixture – All Soluble (*EXT-ALLSOL*)	2.09 (0.41)	1.692	1.692
External Mixture – All Soluble and Surface Active (*EXT-ALLSOL-ST*)	2.39 (0.26)	2.179	2.179
Size-Resolved – External Mixture (*SR-EXT*)	1.10 (0.95)	0.172	0.159

considered, a smaller diameter, $d_{p,c}$, is predicted than the observed. From all the internal mixture scenarios considered, *INT-SALTS* and *INT-ALLSOL* provide the best closure although, $d_{p,c}$ is still underpredicted by 26 and 30 %, respectively. For the external mixture cases, a comparison was done only for the *EXT-ALLSOL* and *EXT-ALLSOL-ST* cases, which were characterized by an underprediction bias. Better closure was achieved for the *EXT-ALLSOL* case, with $d_{p,c}$ being underpredicted by 35 % (Fig. 6b).

The predicted $d_{p,c}$ for each case was then used to determine the theoretical CCN concentration and compared to that measured. As expected from the activation diameter results (Fig. 6), a discrepancy between the predicted and measured CCN concentration was observed for all scenarios within the internal and external mixture cases (Table 2, Fig. 7). The best CCN closure was achieved for the *EXT-AS* where the predicted CCN concentration was found to be ∼20 % greater than the measured CCN concentration. For all other mixing state and chemical composition scenarios, the predicted CCN was approximately twofold greater than measured (Fig. 7). Based on the closure results (Table 2), it is likely that organics contribute some solute and possibly depress surface tension (less than the assumed 25 %) in Atlanta. It is also likely that better closure would be achieved if size-resolved chemical composition were available (Medina et al., 2007). For all the CCN closure analyses performed, a uniform external mixture fraction (equal to $1 - E$ evaluated at dry diameter = 200 nm) was assumed to perform the external CCN closure scenarios. This constitutes an "upper limit" as larger particles tend to be more internally mixed (have a lower $1 - E$; Fig. 8: see Sect. 4.2). As shown in Fig. 8, $1 - E$ does not only change with size, but with time of day, likely from photochemical ageing of particles and mixing of air outside of the boundary layer. The CCN closure for the external mixture scenarios, *EXT-ALLSOL* and *EXT-ALLSOL-ST*, lead to an overestimation and greater discrepancy than their internal mixture counterpart (e.g., *INT-ALLSOL* and *INT-ALLSOL-ST*). This analysis suggests that a more precise knowledge of mixing state (as function of size) as well as chemical composition (size-resolved) is required to achieve closure for complex urban aerosol such as those seen in Atlanta.

The CCN closure errors reported here are higher than reported for other anthropogenically-impacted locations (e.g., Broekhuizen et al., 2006; Medina et al., 2007) but comparable to others sampling externally-mixed aerosol (e.g., Cubison et al., 2008). In all studies, however, best CCN closure was attained with the consideration of size-resolved chemical composition. To assess the impact of size-resolved mixing state on the CCN closure, an additional size-resolved external mixture (*SR-EXT*) scenario was assessed using the mixing state obtained from the fitted CCN activity spectrum over a range of dry diameters (Fig. 8). For *SR-EXT*, the activated or internal mixture fraction (E^*) of the aerosol was assumed to be completely soluble with compositions obtained from

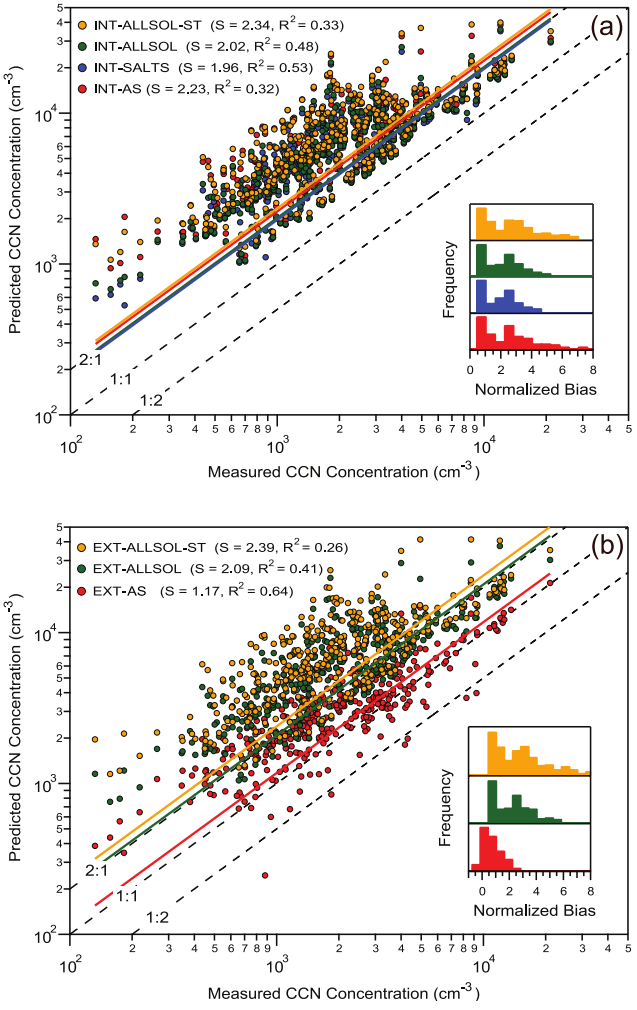

Fig. 7. (a) CCN closure plot for the internal mixture (INT) scenarios. The red, blue, green, and yellow circles correspond to the INT-AS, INT-SALTS, INT-ALLSOL, and INT-ALLSOL-ST cases (Table 1), respectively. **(b)** CCN closure plot for the external mixture (EXT) scenarios. The red, green, and yellow circles correspond to the EXT-AS, EXT-ALLSOL, and EXT-ALLSOL-ST cases, respectively. Inset plots show the observed frequency distribution of the normalized mean bias = $(P_i - O_i)/O_i$.

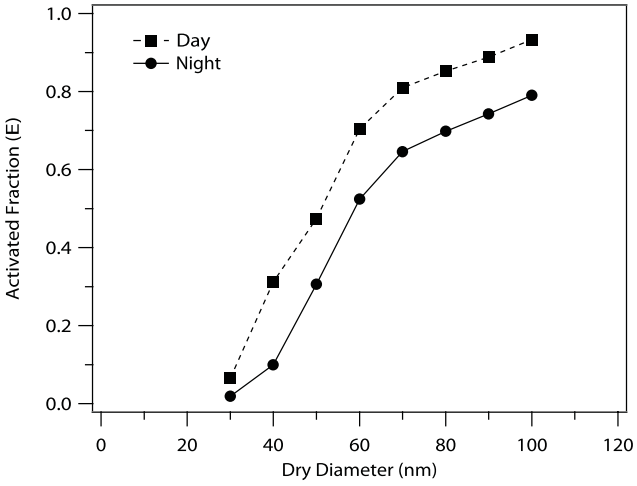

Fig. 8. Example of activation fraction as function of particle size for a day (square) and night (circle) sample. The smaller the particles the more externally mixed they become (smaller E).

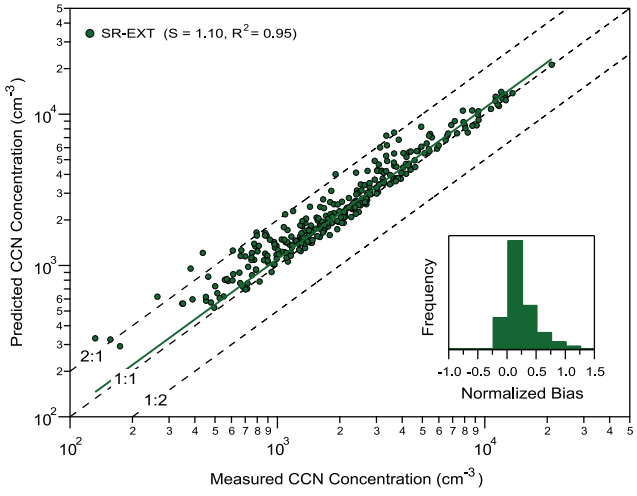

Fig. 9. CCN closure plot for the size-resolved external mixture (SR-EXT) scenario. Inset plot shows the observed frequency distribution of the normalized mean bias = $(P_i - O_i)/O_i$.

the PILS measurements (similar to the *ALLSOL* case above). Predicted N_{CCN} is obtained by applying a modified form of Eq. (9) to find the total CCN concentration at each size bin scaled by the soluble particle fraction:

$$N_{CCN} = \int_{d_{p,c}}^{\infty} \frac{dN_{CCN}}{d\log d_p} E^*_{d_p} d\log d_p \quad (14)$$

where $E^*_{d_p}$ is the internal mixture fraction (E^*) at each diameter d_p. Compared to the internal and external closure scenarios previously discussed, introducing size-resolved mixing state information significantly improves CCN closure (average overprediction = 10 %; Fig. 9), which is approaching the level of agreement seen for very aged aerosol (e.g., Bougiatioti et al., 2011). The residual error is likely due to the assumption of size-averaged composition.

4.2 Mixing state and hygroscopicity time-series

Figure 10 shows the time-series of the sigmoidal fit parameters (E^*, s^*, and C^* in Eq. 2) obtained from fitting the CCN activity spectrum as a function of supersaturation for the 80 nm particles over the entire AMIGAS campaign. The air mass periods discussed in Sect. 2.1 are indicated on the plot. There is no clear correlation between the different periods and fit parameters (Fig. 10); however, there is a slight increase in the non-CCN-active aerosol fraction ($1-E^*$) after

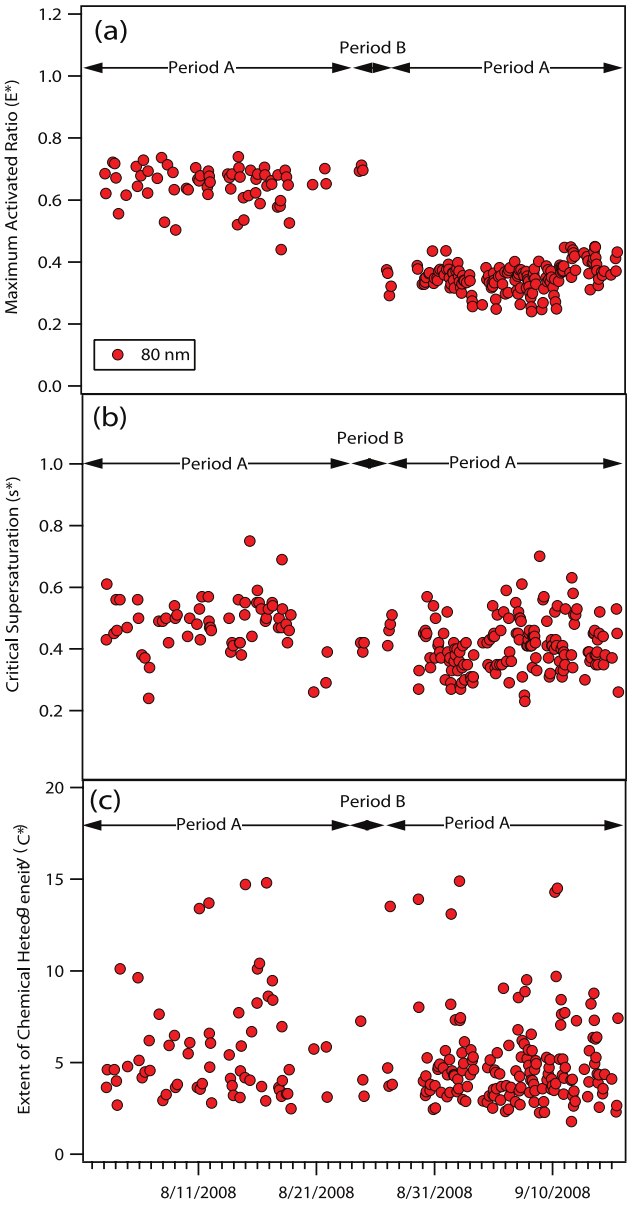

Fig. 10. Time-series of **(a)** maximum activated ratio, **(b)** characteristic critical supersaturation, and **(c)** extent of chemical heterogeneity for 80 nm particles. Period A correspond to air masses originating from the continental US; while period B corresponds to air masses originating from either the Atlantic Ocean or Gulf of Mexico.

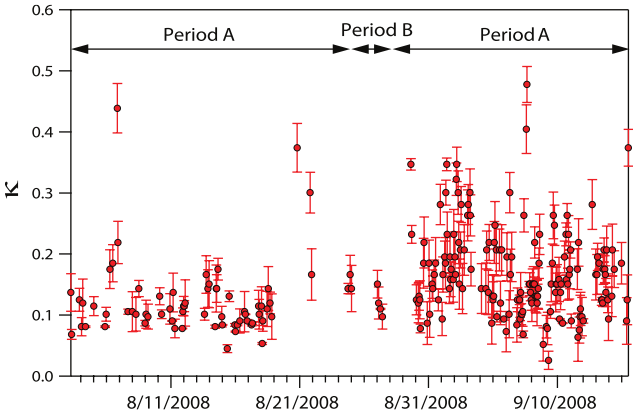

Fig. 11. Time-series of the characteristic hygroscopicity parameter (κ^*; red circles) and its variability (error bars represented by σ_k) for 80 nm particles. Period A correspond to air masses originating from the continental US; while period B corresponds to air masses originating from either the Atlantic Ocean or Gulf of Mexico. Gaps in data are a result of power outage or instrument problems.

27 August (second A Period; Fig. 10a) and a decrease in the characteristic supersaturation (s^*; Fig. 10b). The slight decrease in the s^* (regardless of the increase in the externally mixed aerosol) suggest that the internally mixed particles at the end of the campaign (after 24 August) were slightly more hygroscopic than those observed at the beginning. The increase in the aerosol hygroscopicity may be due to organic compounds reacting in the aqueous phase; therefore increasing the water soluble organic carbon (WSOC) fraction present in the particle phase. This observation is consistent with recent studies (e.g., Hennigan et al., 2008) in Atlanta that found the fraction of the total WSOC in the particle phase to have a strong dependence with RH above 70 % as is the case in this study. As for the chemical heterogeneity of the activated particles (Fig. 10c), the particles have the same chemical variability regardless of the air mass sampled.

κ is calculated using the surface tension of water evaluated at the median column temperature (Petters and Kreidenweis, 2007). However, the surface tension of the CCN can be different from water if surfactants are present (Kiss et al., 2005; Dinar et al., 2007), which can introduce uncertainty in κ calculations (Padró et al., 2010). The κ time-series for the whole AMIGAS campaign for 80 nm particles is shown in Fig. 11, and typically ranged between 0.03–0.48 (mean of 0.16 ± 0.07). These values of κ are consistent with mixtures of soluble salts and organic species (Carrico et al., 2008; Koehler et al., 2009; Petters and Kreidenweis, 2007; Shantz et al., 2008). As for the chemical heterogeneity of the particles, there is no clear correlation between the particle hygroscopicity and air mass sampled. Particles in the 60–100 nm range exhibited similar hygroscopicity, with a κ range for 60 nm between 0.06–0.076 (mean of 0.18 ± 0.09). Smaller particles (40 nm) had on average greater κ, with a range of 0.20–0.92 (mean of 0.3 ± 0.12).

4.3 Droplet activation kinetics

The measured CCN droplet sizes were used to assess the effect of aerosol composition on activation kinetics. In Fig. 12, the droplet size at the point of activation (d_p corresponding to $d_{p,c}$) for a subset of the ambient data is plotted against the instrument supersaturation. The droplet sizes for ambient aerosol are compared to the droplet sizes from $(NH_4)_2SO_4$

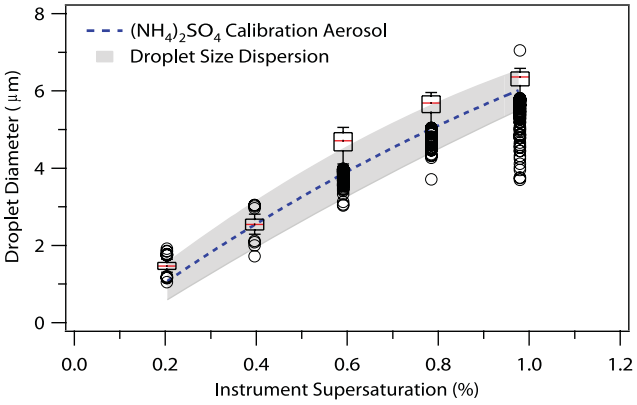

Fig. 12. Droplet growth kinetics study analysis. Box plots for ambient droplet sizes at the point of activation by supersaturation. The whiskers represent the 10th and 90th percentile. Outliers shown as open circles represent those points that are 1.5 times the interquartile range (box width). The dashed blue line corresponds to the $(NH_4)_2SO_4$ calibration droplet size at activation at the same supersaturation. The grey band represents the variability in the average calibration $(NH_4)_2SO_4$ droplet distribution.

calibration aerosol at the same supersaturation. If the droplets formed from ambient CCN are smaller than those from the calibrations, this may indicate that the CCN experience slow growth kinetics from the presence of organics. Special attention should be given to the CCN concentration, as if high enough, it can deplete the water supersaturation in the CFSTGC chamber and explain the reduced droplet sizes (Lathem and Nenes, 2011; Raatikainen et al., 2012). Thus, while threshold growth analysis can rule out the presence of slowly-growing particles, it cannot always unambiguously identify slowly-activating particles. Rather, a detailed numerical model is required to account for the various droplet growth dependencies and numerically constrain kinetic growth parameters (Raatikainen et al., 2012).

During AMIGAS, Atlanta aerosol exhibit similar activation kinetics to $(NH_4)_2SO_4$ (Fig. 12); however, an increase in the number of particles that exhibit smaller droplet sizes was observed at higher supersaturations. The quantity of outliers was shown to increase with supersaturation (e.g., lower activation diameters) from 4 % (at 0.2 % supersaturation) to 9 % (at 1.0 % supersaturation) of the total data points. Of these, some points were found to lie within the variability of the average droplet diameter, especially for the lower supersaturations. A detailed assessment of the few particles that produced small CCN droplet sizes will be the focus of future work.

5 Conclusions

Size-resolved CCN measurements, obtained using Scanning Mobility CCN Analysis, were performed during the AMIGAS campaign in Atlanta, GA, from 1 August until 15 September 2008. Size-resolved CCN activation ratio were used to express the aerosol mixing state (e.g., CCN activation fraction), hygroscopicity, and activation kinetics characteristics. The data were then used to assess CCN closure for a number of chemical composition and mixing state scenarios often taken in atmospheric models to predict CCN concentrations. Of all the cases considered, the best closure was achieved for the size-resolved mixing state scenario (∼10 % overprediction). It is possible that the CCN closure would further improve with detailed size-resolved chemical composition; the improvment in droplet number prediction however will be negligible (e.g., Sotiropoulou et al., 2007; Karydis et al., 2012). The results of the CCN closure scenarios considered here indicate that knowing the chemical composition and mixing state of aerosols allows the accurate prediction (to within 10–20 %) of CCN concentrations. However, for more commonly applied assumptions of aerosol internal mixing, the prediction error can be much higher (100 %), which is consistent with other studies focusing on CCN closure for externally-mixed aerosol (e.g., Cubison et al., 2008; Ervens et al., 2007). As expected, the hygroscopicity parameter of the aerosol exhibits considerable variability over time and particle size, but tends to be 30–50 % lower than the "typical" continental average of 0.3 (Pringle et al., 2010). As for the activated CCN, most of the aerosols sampled during the campaign experienced growth similar to $(NH_4)_2SO_4$ calibration aerosol, suggesting that compositional variability in this region of the world exhibits a minimal impact on CCN activation kinetics. If the same finding applies to other regions of the globe, CCN activation and growth kinetics can be described with one set of kinetic parameters (i.e. uptake coefficient).

Acknowledgements. This research was supported in part by a NASA Earth System Science Fellowship, a DOE GCEP Graduate Research Environmental Fellowship, the Electric Power Research Institute, a NSF-CAREER award and NOAA grants.

Edited by: F. Yu

References

Asa-Awuku, A., Engelhart, G. J., Lee, B. H., Pandis, S. N., and Nenes, A.: Relating CCN activity, volatility, and droplet growth kinetics of β-caryophyllene secondary organic aerosol, Atmos. Chem. Phys., 9, 795–812, doi:10.5194/acp-9-795-2009, 2009.

Asa-Awuku, A., Moore, R. H., Nenes, A., Bahreini, R., Holloway, J. S., Brock, C. A., Middlebrook, A. M., Ryerson, T., Jimenez, J., DeCarlo, P., Hecobian, A., Weber, R., Stickel. R., Tanner, D. J., and Huey, L. G.: Airborne cloud condensation nuclei mea-

surements during the 2006 Texas Air Quality Study, J. Geophys. Res., 116, D11201, doi:10.1029/2010JD014874, 2011.

Bigg, E. K.: Discrepancy between observation and prediction of concentrations of cloud condensation nuclei, Atmos. Res., 20, 82–86, 1986.

Bougiatioti, A., Fountoukis, C., Kalivitis, N., Pandis, S. N., Nenes, A., and Mihalopoulos, N.: Cloud condensation nuclei measurements in the marine boundary layer of the Eastern Mediterranean: CCN closure and droplet growth kinetics, Atmos. Chem. Phys., 9, 7053–7066, doi:10.5194/acp-9-7053-2009, 2009.

Bougiatioti, A., Nenes, A., Fountoukis, C., Kalivitis, N., Pandis, S. N., and Mihalopoulos, N.: Size-resolved CCN distributions and activation kinetics of aged continental and marine aerosol, Atmos. Chem. Phys., 11, 8791–8808, doi:10.5194/acp-11-8791-2011, 2011.

Broekhuizen, K., Chang, R. Y.-W., Leaitch, W. R., Li, S.-M., and Abbatt, J. P. D.: Closure between measured and modeled cloud condensation nuclei (CCN) using size-resolved aerosol compositions in downtown Toronto, Atmos. Chem. Phys., 6, 2513–2524, doi:10.5194/acp-6-2513-2006, 2006.

Butler, A. J., Andrew, M. S., and Russell, A. G.: Daily sampling of $PM_{2.5}$ in Atlanta: Results of the first year of the assessment of spatial aerosol composition in Atlanta study, J. Geophys. Res., 108, 8415, doi:10.1029/2002JD002234, 2003.

Cantrell, W., Shaw, G., Cass, G., Chowdhury, Z., Hughes, L., Prather, K., Guazzotti, S., and Coffee, K.: Closure between aerosol particles and cloud condensation nuclei at Kaashidhoo climate observatory, J. Geophys. Res., 106, 28711–28718, 2001.

Carrico, C. M., Petters, M. D., Kreidenweis, S. M., Collett, J. L., Engling, G., and Malm, W. C.: Aerosol hygroscopicity and cloud droplet activation of extracts of filters from biomass burning experiments, J. Geophys. Res., 113, D08206, doi:10.1029/2007JD009274, 2008.

Cerully, K. M., Raatikainen, T., Lance, S., Tkacik, D., Tiitta, P., Petäjä, T., Ehn, M., Kulmala, M., Worsnop, D. R., Laaksonen, A., Smith, J. N., and Nenes, A.: Aerosol hygroscopicity and CCN activation kinetics in a boreal forest environment during the 2007 EUCAARI campaign, Atmos. Chem. Phys., 11, 12369–12386, doi:10.5194/acp-11-12369-2011, 2011.

Chang, R. Y.-W., Liu, P. S. K., Leaitch, W. R., and Abbatt, J. P. D.: Comparison between measured and predicted CCN concentrations at Egbert, Ontario: Focus on the organic aerosol fraction at a semi-rural site, Atmos. Environ., 41, 8172–8182, 2007.

Chang, R. Y.-W., Slowik, J. G., Shantz, N. C., Vlasenko, A., Liggio, J., Sjostedt, S. J., Leaitch, W. R., and Abbatt, J. P. D.: The hygroscopicity parameter (κ) of ambient organic aerosol at a field site subject to biogenic and anthropogenic influences: relationship to degree of aerosol oxidation, Atmos. Chem. Phys., 10, 5047–5064, doi:10.5194/acp-10-5047-2010, 2010.

Chuang, P., Charlson, R., and Seinfeld, J.: Kinetic limitations on droplet formation in clouds, Nature, 390, 594–596, 1997.

Chuang, P. Y., Collins, D. R., Pawlowska, H., Snider, J. R., Jonsson, H. H., Brenguier, J. L., Flagan, R. C., and Seinfeld, J. H.: CCN measurements during ACE-2 and their relationship to cloud microphysical properties, Tellus, 52B, 843–867, 2000.

Clegg, S. L. and Brimblecombe, P.: Equilibrium partial pressures of strong acids over concentrated saline solutions – I. HNO_3, Atmos. Environ., 22, 91–100, doi:10.1016/0004-6981(88)90302-2, 1988.

Corrigan, C. E. and Novakov, T.: Cloud condensation nucleus activity of organic compounds: a laboratory study, Atmos. Environ., 33, 2661–2668, 1999.

Covert, D., Gras, J., Wiedensohler, A., and Stratmann, F.: Comparison of directly measured CCN with modeled CCN from the number-size distribution in the marine boundary layer during ACE 1 at Cape Grim, Tasmania, J. Geophys. Res., 103, 16597–16608, 1998.

Cruz, C. N. and Pandis, S. N.: A study of the ability of pure secondary organic aerosol to act as cloud condensation nuclei, Atmos. Environ., 31, 2205–2214, 1997.

Cubison, M. J., Ervens, B., Feingold, G., Docherty, K. S., Ulbrich, I. M., Shields, L., Prather, K., Hering, S., and Jimenez, J. L.: The influence of chemical composition and mixing state of Los Angeles urban aerosol on CCN number and cloud properties, Atmos. Chem. Phys., 8, 5649–5667, doi:10.5194/acp-8-5649-2008, 2008.

Dinar, E., Taraniuk, I., Graber, E. R., Anttila, T., Mentel, T. F., and Rudich, Y.: Hygroscopic growth of atmospheric and model humic-like substances, J. Geophys. Res., 112, D05211, doi:10.1029/2006JD007442, 2007.

Dusek, U., Covert, D., Wiedensohler, A., Neususs, C., Weise, D., and Cantrell, W.: Cloud condensation nuclei spectra derived from size distributions and hygroscopic properties of the aerosol in coastal southwest Portugal during ACE-2, Tellus B, 55, 35–53, 2003.

Dusek, U., Frank, G. P., Hildebrandt, L., Curtius, J., Schneider, J., Walter, S., Chand, D., Drewnick, F., Hings, S., Jung, D., Borrmann, S., and Andreae, M. O.: Size matters more than chemistry for cloud-nucleating ability of aerosol particles, Science, 312, 1375–1378, 2006.

Engelhart, G. J., Asa-Awuku, A., Nenes, A., and Pandis, S. N.: CCN activity and droplet growth kinetics of fresh and aged monoterpene secondary organic aerosol, Atmos. Chem. Phys., 8, 3937–3949, doi:10.5194/acp-8-3937-2008, 2008.

Ervens, B., Cubison, M., Andrews, E., Feingold, G., Ogren, J. A., Jimenez, J. L., DeCarlo, P., and Nenes, A.: Prediction of cloud condensation nucleus number concentration using measurements of aerosol size distributions and composition and light scattering enhancement due to humidity, J. Geophys. Res., 112, D10S32, doi:10.1029/2006JD007426, 2007.

Facchini, M. C., Mircea, M., Fuzzi, S., and Charlson, R. J.: Cloud albedo enhancement by surface-active organic solutes in growing droplets, Nature, 401, 257–259, 1999.

Feingold, G. and Chuang, P. Y.: Analysis of the influence of film-forming compounds on droplet growth: Implications for cloud microphysical processes and climate, J. Atmos. Sci., 59, 2006–2018, 2002.

Furutani, H., Dall'osto, M., Roberts, G. C., and Prather, K. A.: Assessment of the relative importance of atmospheric aging on CCN activity derived from field observations, Atmos. Environ., 42, 3130–3142, 2008.

Goldstein, A. H., Koven, C. D., Heald, C. L., and Fung, I.: Biogenic Carbon and Anthropogenic Pollutants Combine to Form a Cooling Haze over the Southeastern US, Proc. Nat. Acad. Sci., 106, 8835–8840, 2009.

Gunthe, S. S., King, S. M., Rose, D., Chen, Q., Roldin, P., Farmer, D. K., Jimenez, J. L., Artaxo, P., Andreae, M. O., Martin, S. T., and Pöschl, U.: Cloud condensation nuclei in pristine tropi-

cal rainforest air of Amazonia: size-resolved measurements and modeling of atmospheric aerosol composition and CCN activity, Atmos. Chem. Phys., 9, 7551–7575, doi:10.5194/acp-9-7551-2009, 2009.

Hartz, K. E. H., Tischuk, J. E., Chan, M. N., Chan, C. K., Donahue, N. M., and Pandis, S. N.: Cloud condensation nuclei activation of limited solubility organic aerosol, Atmos. Environ., 40, 605–617, 2006.

Hennigan, C. J., Bergin, M. H., Dibb, J. E., and Weber, R. J.: Enhanced secondary organic aerosol formation due to water uptake by fine particles, Geophys. Res. Lett., 35, L18801, doi:10.1029/2008GL035046, 2008.

Hennigan, C. J., Bergin, M. H., Russell, A. G., Nenes, A., and Weber, R. J.: Gas/particle partitioning of water-soluble organic aerosol in Atlanta, Atmos. Chem. Phys., 9, 3613–3628, doi:10.5194/acp-9-3613-2009, 2009.

Irwin, M., Robinson, N., Allan, J. D., Coe, H., and McFiggans, G.: Size-resolved aerosol water uptake and cloud condensation nuclei measurements as measured above a Southeast Asian rainforest during OP3, Atmos. Chem. Phys., 11, 11157–11174, doi:10.5194/acp-11-11157-2011, 2011.

Kammermann, L., Gysel, M., Weingartner, E., Herich, H., Cziczo, D. J., Holst, T., Svenningson, B., Arneth, A., and Baltensperger, U.: Sub-arctic atmospheric aerosol composition 3: Measured and modeled properties of cloud condensation nuclei (CCN), J. Geophys. Res., 115, D04202, doi:10.1029/2009JD012447, 2010.

Karydis, V. A., Capps, S. L., Russell, A. G., and Nenes, A.: Adjoint sensitivity of global cloud droplet number to aerosol and dynamical parameters, Atmos. Chem. Phys., 12, 9041–9055, doi:10.5194/acp-12-9041-2012, 2012.

Kiss, G., Tombacz, E., and Hansson, H. C.: Surface tension effects of humic-like substances in the aqueous extract of tropospheric fine aerosol, J. Atmos. Chem., 50, 279–294, 2005.

Koehler, K. A., Kreidenweis, S. M., DeMott, P. J., Petters, M. D., Prenni, A. J., and Carrico, C. M.: Hygroscopicity and cloud droplet activation of mineral dust aerosol, Geophys. Res. Lett., 36, L08805, doi:10.1029/2009GL037348, 2009.

Köhler, H.: The nucleus in and the growth of hygroscopic droplets, Trans. Faraday Soc., 32, 1152–1161, 1936.

Kuwata, M., Kondo, Y., Miyazaki, Y., Komazaki, Y., Kim, J. H., Yum, S. S., Tanimoto, H., and Matsueda, H.: Cloud condensation nuclei activity at Jeju Island, Korea in spring 2005, Atmos. Chem. Phys., 8, 2933–2948, doi:10.5194/acp-8-2933-2008, 2008.

Lance, S.: Quantifying compositional impacts of ambient aerosol on cloud droplet formation, Doctoral Thesis, Georgia Institute of Technology, USA, 2007.

Lance, S., Nenes, A., and Rissman, T.: Chemical and dynamical effects on cloud droplet number: Implications for estimates of the aerosol indirect effect, J. Geoph. Res., 109, D22208, doi:10.1029/2004JD004596, 2004.

Lance, S., Medina, J., Smith, J. N., and Nenes, A.: Mapping the operation of the DMT continuous flow CCN counter, Aerosol Sci. Tech., 40, 242–254, 2006.

Lance, S., Nenes, A., Mazzoleni, C., Dubey, M., Gates, H., Varutbangkul, V., Rissman, T. A., Murphy, S. M., Sorooshian, A., Brechtel, F., Flagan, R. C., Seinfeld, J. H., Feingold, G., and Jonsson, H.: CCN Activity, Closure and Droplet Growth Kinetics of Houston Aerosol During the Gulf of Mexico Atmospheric Composition and Climate Study (GoMACCS), J. Geophys. Res., 114, D00F15, doi:10.1029/2008JD011699, 2009.

Lance, S., Raatikainen, T., Onasch, T., Worsnop, D. R., Yu, X.-Y., Alexander, M. L., Stolzenburg, M. R., McMurry, P. H., Smith, J. N., and A. Nenes, Aerosol mixing-state, hygroscopic growth and cloud activation efficiency during MIRAGE 2006, Atmos. Chem. Phys. Discuss., 12, 15709–15742, doi:10.5194/acpd-12-15709-2012, 2012.

Lathem, T. L. and Nenes, A.: Water vapor depletion in the DMT Continuous Flow CCN Chamber: effects on supersaturation and droplet growth, Aerosol Sci. Technol., 45, 604–615, doi:10.1080/02786826.2010.551146, 2011.

Li, Z. D., Williams, A. L., and Rood, M. J.: Influence of soluble surfactant properties on the activation of aerosol particles containing inorganic solute, J. Atmos. Sci., 55, 1859–1866, 1998.

Lim, H.-J. and Turpin, B. J.: Origins of primary and secondary organic aerosol in Atlanta: Results of time-resolved measurements during the Atlanta Supersite Experiment, Environ. Sci. Technol., 36, 4489–4496, 2002.

Liu, P., Leaitch, W., Banic, C., Li, S., Ngo, D., and Megaw, W.: Aerosol observations at Chebogue Point during the 1993 North Atlantic Regional Experiment: Relationships among cloud condensation nuclei, size distribution, and chemistry, J. Geophys. Res., 101, 28971–28990, 1996.

McMurry, P. H., Wang, X., Park, K., and Ehara, K.: The relationship between mass and mobility for atmospheric particles: A new technique for measuring particle density, Aerosol Sci. Tech., 36, 227–238, 2002.

Medina, J., Nenes, A., Sotiropoulou, R. E. P., Cottrell, L. D., Ziemba, L. D., Beckman, P. J., and Griffin, R. J.: Cloud condensation nuclei closure during the International Consortium for Atmospheric Research on Transport and Transformation 2004 campaign: Effects of size-resolved composition, J. Geophys. Res., 112, D10S31, doi:10.1029/2006JD007588, 2007.

Mochida, M., Nishita-Hara, C., Kitamori, Y., Aggarwal, S. G., Kawamura, K., Miura, K., and Takami, A.: Size-segregated measurements of cloud condensation nucleus activity and hygroscopic growth for aerosols at Cape Hedo, Japan, in spring 2008, J. Geophys. Res., 115, D21207, doi:10.1029/2009JD013216, 2010.

Moore, R., Nenes, A., and Medina, J.: Scanning Mobility CCN Analysis – A method for fast measurements of size resolved CCN distributions and activation kinetics, Aerosol Sci. Technol., 44, 861–871, 2010.

Moore, R. H., Bahreini, R., Brock, C. A., Froyd, K. D., Cozic, J., Holloway, J. S., Middlebrook, A. M., Murphy, D. M., and Nenes, A.: Hygroscopicity and composition of Alaskan Arctic CCN during April 2008, Atmos. Chem. Phys., 11, 11807–11825, doi:10.5194/acp-11-11807-2011, 2011.

Moore, R. H., Raatikainen, T., Langridge, J. M., Bahreini, R., Brock, C. A., Holloway, J. S., Lack, D. A., Middlebrook, A. M., Perring, A. E., Schwarz, J. P., Spackman J. R., and Nenes, A.: CCN Spectra, Hygroscopicity, and Droplet Activation Kinetics of Secondary Organic Aerosol Resulting from the 2010 Deepwater Horizon Oil Spill, Environ. Sci. Technol., 46, 3093–3100, doi:10.1021/es203362w, 2012.

Murphy, S. M., Agrawal, H., Sorooshian, A., Padro, L. T., Gates, H., Hersey, S., Welch, W. A., Jung, H., Miller, J. W., Cocker III, D. R., Nenes, A., Jonsson, H. H., Flagan, R. C., and Seinfeld, J. H.:

Comprehensive simultaneous shipboard and airborne characterization of exhaust from a modern container ship at sea, Environ. Sci. Tech., 43, 4626–4640, doi:10.1021/es802413j, 2009.

Nenes, A., Pilinis, C., and Pandis, S. N.: ISORROPIA: A new thermodynamic model for multiphase multicomponent inorganic aerosols, Aquat. Geochem., 4, 123–152, 1998.

Nenes, A., Ghan, S., Abdul-Razzak, H., Chuang, P. Y., and Seinfeld, J. H.: Kinetic limitations on cloud droplet formation and impact on cloud albedo, Tellus, 53B, 133–149, 2001.

Padró, L. T., Asa-Awuku, A., Morrison, R., and Nenes, A.: Inferring thermodynamic properties from CCN activation experiments: single-component and binary aerosols, Atmos. Chem. Phys., 7, 5263–5274, doi:10.5194/acp-7-5263-2007, 2007.

Padró, L. T., Tkacik, D. T., Lathem, T., Hennigan, C. J., Sulivan, A. P., Weber, R. J., Huey, L. G., and Nenes, A.: Investigation of cloud condensation nuclei properties and droplet growth kinetics of the water-soluble aerosol fraction in Mexico City, J. Geophys. Res., 115, D09204, doi:10.1029/2009JD013195, 2010.

Petters, M. D. and Kreidenweis, S. M.: A single parameter representation of hygroscopic growth and cloud condensation nucleus activity, Atmos. Chem. Phys., 7, 1961–1971, doi:10.5194/acp-7-1961-2007, 2007.

Petters, M. D., Kreidenweis, S. M., Prenni, A. J., Sullivan, R. C., Carrico, C. M., Koehler, K. A., and Ziemann, P. J.: Role of molecular size in cloud droplet activation, Geophys. Res. Lett., 36, L22801, doi:10.1029/2009GL040131, 2009.

Pilinis, C. and Seinfeld, J. H.: Continued development of a general equilibrium-model for inorganic multicomponent atmospheric aerosols, Atmos. Environ., 21, 2453–2466, 1987.

Pitzer, K. S. and Mayorga, G.: Thermodynamics of electrolytes-II. Activity and osmotic coefficients for strong electrolytes with one or both ions univalent, J. Phys. Chem., 77, 2300–2308, 1973.

Pringle, K. J., Tost, H., Pozzer, A., Pöschl, U., and Lelieveld, J.: Global distribution of the effective aerosol hygroscopicity parameter for CCN activation, Atmos. Chem. Phys., 10, 5241–5255, doi:10.5194/acp-10-5241-2010, 2010.

Quinn, P. K., Bates, T. S., Coffman, D. J., and Covert, D. S.: Influence of particle size and chemistry on the cloud nucleating properties of aerosols, Atmos. Chem. Phys., 8, 1029–1042, doi:10.5194/acp-8-1029-2008, 2008.

Raatikainen, T., Moore, R. H., Lathem, T. L., and Nenes, A.: A coupled observation – modeling approach for studying activation kinetics from measurements of CCN activity, Atmos. Chem. Phys., 12, 4227–4243, doi:10.5194/acp-12-4227-2012, 2012.

Raymond, T. M. and Pandis, S. N.: Cloud activation of single-component organic aerosol particles, J. Geophys. Res., 107, 4787, doi:10.1029/2002JD002159, 2002.

Rhoads, K. P., Phares, D. J., Wexler, A., and Johnston, M. V.: Size-resolved ultrafine particle composition analysis, 1, Atlanta, J. Geophys. Res., 108, 8418, doi:10.1029/2001JD001211, 2003.

Rissler, J., Swietlicki, E., Zhou, J., Roberts, G., Andreae, M. O., Gatti, L. V., and Artaxo, P.: Physical properties of the submicrometer aerosol over the Amazon rain forest during the wet-to-dry season transition – comparison of modeled and measured CCN concentrations, Atmos. Chem. Phys., 4, 2119–2143, doi:10.5194/acp-4-2119-2004, 2004.

Rissman, T., Nenes, A., and Seinfeld, J. H.: Chemical amplification (or dampening) of te Twomey effect: Conditions derived from droplet activation theory, J. Atmos. Sci., 61, 919–930, 2004.

Rissman, T. A., VanReken, T. M., Wang, J., Gasparini, R., Collins, D. R., Jonsson, H. H., Brechtel, F. J., Flagan, R. C., and Seinfeld, J. H.: Characterization of ambient aerosol from measurements of cloud condensation nuclei during the 2003 Atmospheric Radiation Measurement Aerosol Intensive Observational Period at the Southern Great Plains site in Oklahoma, J. Geophys. Res., 111, D05S11, doi:10.1029/2004JD005695, 2006.

Roberts, G., Mauger, G., Hadley, O., and Ramanathan, V.: North American and Asian aerosols over the eastern Pacific Ocean and their role in regulating cloud condensation nuclei, J. Geophys. Res., 111, D13205, doi:10.1029/2005JD006661, 2006.

Roberts, G. C. and Nenes, A.: A continuous-flow streamwise thermal-gradient CCN chamber for atmospheric measurements, Aerosol Sci. Technol., 39, 206–211, 2005.

Roberts, G. C., Artaxo, P., Zhou, J., Swietlicki, E., and Andreae, M. O.: Sensitivity of CCN spectra on chemical and physical properties of aerosol: A case study from the Amazon Basin, J. Geophys. Res., 107, 8070, doi:10.1029/2001JD000583, 2002.

Roberts, G. C., Nenes, A., Seinfeld, J. H., and Andreae, M. O.: Impact of biomass burning on cloud properties in the Amazon Basin, J. Geophys. Res., 108, 4062, doi:10.1029/2001JD000985, 2003.

Roberts, G. C., Day, D. A., Russell, L. M., Dunlea, E. J., Jimenez, J. L., Tomlinson, J. M., Collins, D. R., Shinozuka, Y., and Clarke, A. D.: Characterization of particle cloud droplet activity and composition in the free troposphere and the boundary layer during INTEX-B, Atmos. Chem. Phys., 10, 6627–6644, doi:10.5194/acp-10-6627-2010, 2010.

Rose, D., Gunthe, S. S., Mikhailov, E., Frank, G. P., Dusek, U., Andreae, M. O., and Pöschl, U.: Calibration and measurement uncertainties of a continuous-flow cloud condensation nuclei counter (DMT-CCNC): CCN activation of ammonium sulfate and sodium chloride aerosol particles in theory and experiment, Atmos. Chem. Phys., 8, 1153–1179, doi:10.5194/acp-8-1153-2008, 2008.

Rose, D., Nowak, A., Achtert, P., Wiedensohler, A., Hu, M., Shao, M., Zhang, Y., Andreae, M. O., and Pöschl, U.: Cloud condensation nuclei in polluted air and biomass burning smoke near the mega-city Guangzhou, China – Part 1: Size-resolved measurements and implications for the modeling of aerosol particle hygroscopicity and CCN activity, Atmos. Chem. Phys., 10, 3365–3383, doi:10.5194/acp-10-3365-2010, 2010.

Rose, D., Gunthe, S. S., Su, H., Garland, R. M., Yang, H., Berghof, M., Cheng, Y. F., Wehner, B., Achtert, P., Nowak, A., Wiedensohler, A., Takegawa, N., Kondo, Y., Hu, M., Zhang, Y., Andreae, M. O., and Pöschl, U.: Cloud condensation nuclei in polluted air and biomass burning smoke near the mega-city Guangzhou, China – Part 2: Size-resolved aerosol chemical composition, diurnal cycles, and externally mixed weakly CCN-active soot particles, Atmos. Chem. Phys., 11, 2817–2836, doi:10.5194/acp-11-2817-2011, 2011.

Ruehl, C. R., Chuang, P. Y., and Nenes, A.: How quickly do cloud droplets form on atmospheric particles?, Atmos. Chem. Phys., 8, 1043–1055, doi:10.5194/acp-8-1043-2008, 2008.

Ruehl, C. R., Chuang, P. Y., and Nenes, A.: Distinct CCN activation kinetics above the marine boundary layer along the California coast, Geophys. Res. Lett., 36, L15814, doi:10.1029/2009GL038839, 2009.

Shantz, N. C., Leaitch, W. R., Phinney, L., Mozurkewich, M., and Toom-Sauntry, D.: The effect of organic compounds on the growth rate of cloud droplets in marine and forest settings, Atmos. Chem. Phys., 8, 5869–5887, doi:10.5194/acp-8-5869-2008, 2008.

Snider, J., Guibert, S., Brenguier, J., and Putaud, J.: Aerosol activation in marine stratocumulus clouds: 2. Köhler and parcel theory closure studies, J. Geophys. Res., 108, 8629, doi:10.1029/2002JD002692, 2003.

Solomon, P. A., Chameides, W., Weber, R., Middlebrook, A., Kiang, C. S., Russell, A. G., Butler, A., Turpin, B., Mikel, D., Scheffe, R., Cowling, E., Edgerton, E., St. John, J., Jansen, J., McMurry, P., Hering, S., and Bahadori, T.: Overview of the 1999 Atlanta Supersite Project, J. Geophys. Res., 108, 8413, doi:10.1029/2001JD001458, 2003.

Sorooshian, A., Murphy, S. M., Hersey, S., Gates, H., Padro, L. T., Nenes, A., Brechtel, F. J., Jonsson, H., Flagan, R. C., and Seinfeld, J. H.: Comprehensive airborne characterization of aerosol from a major bovine source, Atmos. Chem. Phys., 8, 5489–5520, doi:10.5194/acp-8-5489-2008, 2008.

Sotiropoulou, R. E. P., Nenes, A., Adams, P. J., and Seinfeld, J. H.: Cloud condensation nuclei prediction error from application of Köhler theory: Importance for the aerosol indirect effect, J. Geophys. Res., 112, D12202, doi:10.1029/2006JD007834, 2007.

Stroud, C. A., Nenes, A., Jimenez, J. L., DeCarlo, P. F., Huffman, J. A., Bruintjes, R., Nemitz, E., Delia, A. E., Toohey, D. W., Guenther, A. B., and Nandi, S.: Cloud activating properties of aerosol observed during CELTIC, J. Atmos. Sci., 64, 441–459, 2007.

Sullivan, A. P., Weber, R. J., Clements, A. L., Turner, J. R., Bae, M. S., and Schauer, J. J.: A method for on-line measurement of water-soluble organic carbon in ambient aerosol particles: Results from an urban site, Geophys. Res. Lett., 31, L13105, doi:10.1029/2004GL019681, 2004.

Su, H., Rose, D., Cheng, Y. F., Gunthe, S. S., Massling, A., Stock, M., Wiedensohler, A., Andreae, M. O., and Pöschl, U.: Hygroscopicity distribution concept for measurement data analysis and modeling of aerosol particle mixing state with regard to hygroscopic growth and CCN activation, Atmos. Chem. Phys., 10, 7489–7503, doi:10.5194/acp-10-7489-2010, 2010.

Twomey, S.: Minimum size of particle for nucleation in clouds, J. Atmos. Sci., 34, 1832–1835, 1977.

VanReken, T. M., Rissman, T. A., Roberts, G. C., Varutbangkul, V., Jonsson, H. H., Flagan, R. C., and Seinfeld, J. H.: Toward aerosol/cloud condensation nuclei (CCN) closure during CRYSTAL-FACE, J. Geophys. Res., 108, 4633, doi:10.1029/2003JD003582, 2003.

Vestin, A., Rissler, J., Swietlicki, E., Frank, G. P., and Andreae, M. O.: Cloud-nucleating properties of the Amazonian biomass burning aerosol: Cloud condensation nuclei measurements and modeling, J. Geophys. Res., 112, D14201, doi:10.1029/2006JD008104, 2007.

Wang, J.: Effects of spatial and temporal variations in aerosol properties on mean cloud albedo, J. Geophys. Res., 112, D16201, doi:10.1029/2007JD008565, 2007.

Wang, J., Lee, Y.-N., Daum, P. H., Jayne, J., and Alexander, M. L.: Effects of aerosol organics on cloud condensation nucleus (CCN) concentration and first indirect aerosol effect, Atmos. Chem. Phys., 8, 6325–6339, doi:10.5194/acp-8-6325-2008, 2008.

Wang, J., Cubison, M. J., Aiken, A. C., Jimenez, J. L., and Collins, D. R.: The importance of aerosol mixing state and size-resolved composition on CCN concentration and the variation of the importance with atmospheric aging of aerosols, Atmos. Chem. Phys., 10, 7267–7283, doi:10.5194/acp-10-7267-2010, 2010.

Weber, R., Bergin, M., Kiang, C. S., Chameides, W., Orsini, D., St, J. J., Chang, M, Carrico, C., Lee, Y. N., Dasgupta, P., Slanina, J., Turpin, B., Edgerton, E., Hering, S., Allen, G., and Solomon, P.: Short-Term Temporal Variation In PM2.5 Mass And Chemical Composition During The Atlanta Supersite Experiment, 1999, J. Air Waste Manage. Assoc., 53, 84–91, 2003.

Weber, R. J., Orsini, D., Daun, Y., Lee, Y. N., Klotz, P. J., and Brechtel, F.: A particle-into-liquid collector for rapid measurement of aerosol bulk chemical composition, Aerosol Sci. Tech., 35, 718–727, 2001.

Weber, R. J., Sullivan, A. P., Peltier, R. E., Russell, A., Yan, B., Zheng, M., de Gouw, J., Warneke, C., Brock, C., Holloway, J. S., Atlas, E. L., and Edgerton, E.: A study of secondary organic aerosol formation in the anthropogenic-influenced southeastern United States, J. Geophys. Res.-Atmos., 112, D13302, doi:10.1029/2007JD008408, 2007.

Yum, S. S., Roberts, G., Kim, J. H., Song, K., and Kim, D.: Submicron aerosol size distributions and cloud condensation nuclei concentrations measured at Gosan, Korea, during the Atmospheric Brown Clouds – East Asian Regional Experiment 2005, J. Geophys. Res., 112, D22S32, doi:10.1029/2006JD008212, 2007.

Zhou, J., Swietlicki, E., Berg, O. H., Aalto, P. P., Hämeri, K., Nilsson, E. D., and Leck, C.: Hygroscopic properties of aerosol particles over the central Arctic Ocean during summer, J. Geophys. Res., 106, 32111–32123, 2001.